Determination of the Nature of the Heme Environment in Nitrosyl Indoleamine 2,3-Dioxygenase Using Multiple-Scattering Analyses of X-ray Absorption Fine Structure†

Jade B. Aitken,‡ Sushila E. Thomas,‡ Roland Stocker,§ Shane R. Thomas,§ Osamu Takikawa,|| Robert S. Armstrong,*,‡ and Peter A. Lay*,‡

Centre for Structural Biology and Structural Chemistry, and Centre for Heavy Metals Research, School of Chemistry, The University of Sydney, New South Wales 2006, Australia, The Heart Research Institute, 145 Missenden Road, Camperdown New South Wales 2050, Australia, and Department of Pharmacology, Hokkaido University, Sapporo 060-8638, Japan

Received February 17, 2004; Revised Manuscript Received March 29, 2004

ABSTRACT: Multiple-scattering analysis of X-ray absorption fine structure data on the NO adducts of indoleamine 2,3-dioxygenase (IDO) and analysis of X-ray absorption near-edge structure (XANES) have provided the first direct structural information about the iron center for this ubiquitous mammalian metalloprotein. The $IDO^{II}NO$ adduct, which is likely to play a physiological role in the immune system, differs from similar adducts such as $Mb^{II}NO$ and $Lb^{II}NO$ in that the Fe−His bond is essentially broken. At 10 K, the Fe−N_p(av) bond length = 2.00(2) Å, Fe−NO bond length = 1.75 Å, and angle = 140°, which are typical of five-coordinate $Fe^{II}NO$ species. The XANES is also closer to that of five-coordinate model complexes than six-coordinate species. In addition to the $Fe^{II}NO$ species, there was a minor component of the $Fe^{III}NO$ adduct because of incomplete reduction of the Fe^{II} species. This was also a five-coordinate center and consists of a linear $Fe^{II}NO^{+}$ moiety with the Fe−N_p(av) bond length = 2.00(2) Å, Fe−NO bond length = 1.63(3) Å, and angle = 179°. The results indicate that both the blocking of the heme site to O_2 binding and conformational changes induced by breaking the Fe−N_ϵ bond may be important mechanisms by which NO inhibits IDO in vitro and in vivo.

Indoleamine 2,3-dioxygenase (IDO)[1] is a monomeric glycoprotein (40−45 kDa) containing 0.8 mol of protoporphyrin IX per mole of enzyme (*1*−*3*). In its native ferric form, IDO is inactive and requires reductive activation (*4*, *5*). Once in its active ferrous form, IDO has a high affinity for its main substrate, tryptophan (Trp) that becomes oxidized to *N*-formylkynurenine. Both the Fe^{III} and Fe^{II} forms of IDO have been studied in vivo and in vitro. Spectroscopic evidence to date has shown that IDO is similar to typical monomeric heme proteins such as myoglobin (Mb) and leghemoglobin (Lb) (*6*−*9*). As such, IDO is expected to exhibit properties in common with other heme proteins having similar coordination environments. IDO displays ligand binding properties and a pH dependence, analogous to those of Mb (*1*, *3*).

IDO is found in various tissues (*2*). In rabbits, the highest levels of IDO are found in the small intestine, lung, and colon, while in mice it is located mainly in the epididymus, colon, and small intestine (*1*). In humans, it is present mostly in the lung, small intestine, and placenta (*1*). The enzyme can be induced in many different cells, including mononuclear phagocytes, endothelial cells, and neoplastic cell lines (*10*). The principal inducer of IDO, both in vitro and in vivo, is interferon-γ (IFN_γ) (*2*, *11*, *12*), and certain activities of IFN_γ, such as antimicrobial and antiproliferative activity, are associated with the induction of IDO and the subsequent local depletion of Trp (*2*, *10*−*12*).

Without a bound substrate, native ferric IDO, like Lb, is a mixture of high-spin/low-spin states at room temperature,

† This research was carried out at the Stanford Synchrotron Radiation Laboratory (SSRL), a National User Facility operated by Stanford University on behalf of the U.S. Department of Energy, Office of Basic Energy Sciences. The SSRL Structural Molecular Biology Program is supported by the Department of Energy, Office of Biological and Environmental Research and by the National Institutes of Health, National Centre for Research Resources, Biomedical Technology Program. The authors (P.A.L. and R.S.A.) are grateful for funding from the Australian Research Council (ARC institutional and discovery grants), the University of Sydney (Sesqui R and D grant), and the Access to Major Facilities Program funded by the Department of Industry, Science and Resources and managed by the Australian Nuclear Science and Technology Organization. This work was supported by a grant-in-aid from the National Health and Medical Research Council of Australia (NHMRC), and R.S. is a recipient of a NH and MRC Senior Principal Research Fellowship.

* To whom correspondence should be addressed. E-mail: p.lay@chem.usyd.edu.au (P.A.L.); r.armstrong@chem.usyd.edu.au (R.S.A.).

‡ The University of Sydney.

§ The Heart Research Institute; Current address: Centre for Vascular Research, School of Medical Sciences, University of New South Wales, and Department of Haematology, Prince of Wales Hospital, University of New South Wales, Sydney, New South Wales 2052, Australia,

|| Hokkaido University.

[1] Abbreviations: CD, circular dichroism; Hb, hemoglobin; IDO, indolamine 2,3-dioxygenase; IFN_γ, interferon-γ; Lb, leghemoglobin; Mb, myoglobin; MCD, magnetic circular dichroism; MS, multiple scattering; NOS, nitric oxide synthase; SSRL, Stanford Synchrotron Research Laboratory; TPP, *meso*-tetraphenylporphyrinato(2−); XAFS, X-ray absorption fine structure; XANES, X-ray absorption near-edge structure.

10.1021/bi049645s CCC: $27.50
Published on Web 04/09/2004

with the proportion of low-spin heme increasing as the temperature is decreased (*4*). It has been suggested that the sixth-coordination site of low-spin *met*-IDO is occupied by a distorted imidazole (*4*), while in the high-spin form it is replaced by an aqua ligand, which occurs in other heme proteins (*13*). The ferrous form of IDO exhibits a high-spin absorption spectrum in both free and substrate-bound conditions (*4*). Like Lb (*14*−*16*), IDO appears to have a much larger heme pocket than Mb, as indicated by electronic absorption spectroscopy (UV/Vis), circular (CD) and magnetic circular dichroism (MCD) studies, and the fact that IDO also binds large ligands, such as norharman and 4-phenylpyridine (*7*, *10*). The presence of a relatively large pocket is possibly attributable to a requirement to accommodate the large Trp substrate into the heme cavity. Despite the interest in this important mammalian heme protein, IDO and its adducts have defied many attempts to obtain structures by protein crystallography and NMR spectroscopy.

Nitric oxide (NO) adducts of IDO are believed to be involved in the modulation of the catalytic activity of this heme protein. NO is an important signal and effector molecule in the body and as such is involved in the immune, nervous, and vascular systems. Nitric oxide is generated via oxidative metabolism of L-arginine (Arg) catalyzed by nitric oxide synthase (NOS) (*12*). In the vasculature, NO acts on soluble guanylyl cyclase in smooth muscle cells and thereby plays a key role in vascular relaxation (*17*). Nitric oxide also plays a role in the vasodilatory response observed in victims of the insect *Rhodnius prolixus* (*18*) and is found in the human lung as *S*-nitrosylated Hb (*19*). Nitric oxide reacts rapidly with heme proteins, and this can result in either activation or inhibition of enzyme activity (*12*, *19*−*21*). Recently, it has been found that there is a similarity and possibly a functional relationship between the Arg and Trp metabolic pathways, which are initiated by NOS and IDO, respectively (*12*). For example, NO inhibits IDO in vitro, and it is postulated that it regulates IDO activity in vivo (*10*).

Here, the structure of the active site of the $Fe^{II}NO$ adduct of IDO has been probed by multiple-scattering (MS) analyses of the K-edge Fe X-ray absorption fine structure (XAFS). This is the first structural determination of a heme site in IDO or its adducts. MS analyses of XAFS data have been used successfully for studies of the structural detail of the active sites of the NO adducts of Mb (*20*) and Lb (*22*).

EXPERIMENTAL PROCEDURES

General Procedures. met-IDO was prepared according to methods published previously (*23*), and the concentration (2.6 mM, $\epsilon_{406} = 160\ mM^{-1}\ cm^{-1}$) and integrity of *met*-IDO were confirmed by UV/Vis spectroscopy (prior to conversion to the nitrosylated protein). All manipulations of the protein were performed in protein-clean glassware. Prior to use, all glassware was rinsed with Milli-Q water. $IDO^{II}NO$ was prepared by a standard method for the production of $Fe^{II}NO$ compounds used previously for $Mb^{II}NO$ (*24*). This involved adding a stoichiometric amount of nitrite to the deoxygenated *met*-IDO sample, followed by an excess of dithionite, which nitrosylated and reduced the sample at the heme center. The reaction occurred over ∼30−45 min and was accompanied by a color change from the brown *met*-IDO to the red $IDO^{II}NO$. The sample was subsequently diluted with glycerol to produce a 40% (v/v) glycerol/aqueous solution to protect the protein and form a glass upon freezing. This solution had a final IDO−NO concentration of 1.6 mM. The solution was syringed into 140-μL Lucite XAFS cells (23 × 2 × 3 mm) with 63.5-μm-thick Mylar tape windows. The solutions were frozen in a liquid N_2/*n*-hexane slush bath to form a homogeneous glass, and the frozen solutions were stored in liquid N_2 prior to inserting them into the liquid He cryostat for data collection.

UV−*Vis Spectroscopy.* The integrity of the sample of the $IDO^{II}NO$ adduct was determined by UV/Vis spectroscopy prior to X-ray absorption spectroscopy (XAS) studies. The UV/Vis spectra of the met precursor and the IDO−NO sample were recorded at the Stanford Synchrotron Radiation Laboratories (SSRL) using a Hewlett-Packard 8452A Diode Array spectrophotometer with a wavelength resolution of 2 nm.

XAS Data Collection. The iron K-edge X-ray absorption spectra of the IDO adducts were recorded at SSRL on beamline 9−3. Beamline 9−3 uses a focused beamline, and the monochromator was detuned 50% and defocused to reduce photodamage from the focused beam. Data were collected as fluorescence spectra, using a Canberra 30-element Ge detector. The samples were held at a temperature of 10 K using an Oxford Instruments continuous-flow liquid helium cryostat. The sample was mounted at a 45° incidence, and the detector viewed the sample fluorescence at 90°, relative to the incident X-ray beam. A calibration channel with an Fe foil was used to account for the energy shifts in the monochromator. For each sample, 12−20 scans were recorded. During the collection of data, the edge of each XAS spectrum was monitored for photodecomposition.

XAFS Model. The porphyrin fragment was modeled in two-dimensional space (*20*) and with 4-fold symmetry (Figure 1). A number of single- and mixed-site models was considered for $IDO^{II}NO$. The initial model consisted of a six-coordinate heme group with NO as the distal ligand and the imidazole ring of histidine as the proximal axial ligand as described previously (*20*, *22*, *25*). Several mixed-site models were considered; in the first site, there was a variation of the $Fe-N_\epsilon$ bond length (starting positions of 2.0, 2.1, and 2.5 Å). The second site in the mixed-site model was one of the following: a five-coordinate NO heme protein with the proximal position empty; a 2.5-Å proximal axial ligand distance (in conjunction with a 2.0-Å distance in the first site); or a 2.0-Å proximal axial ligand distance (in conjunction with a 2.5-Å distance in the first site). When mixed-site models were used, the two porphyrin groups were constrained to be identical, consistent with the similar $Fe-N_p$ bond lengths in all heme−NO adducts (*20*, *26*, *27*). This improved the determinacy, and the two sites were set 15 Å apart to ensure that no interactions occurred between the two heme groups during calculations of the XAFS in the fitting process. A complete set of restraints and constraints for these models is contained in the Supporting Information (Table S1), where σ_{res} is analogous to the estimated standard deviation.

XFIT Data Analysis. MS analyses of XAFS data were performed using XFIT, which employs a nonlinear least-squares fitting of the XAFS spectrum, through the minimization of the sum of the square of the residuals (*20*, *28*). XFIT integrates FEFF6.01 in its model fitting calculations, which

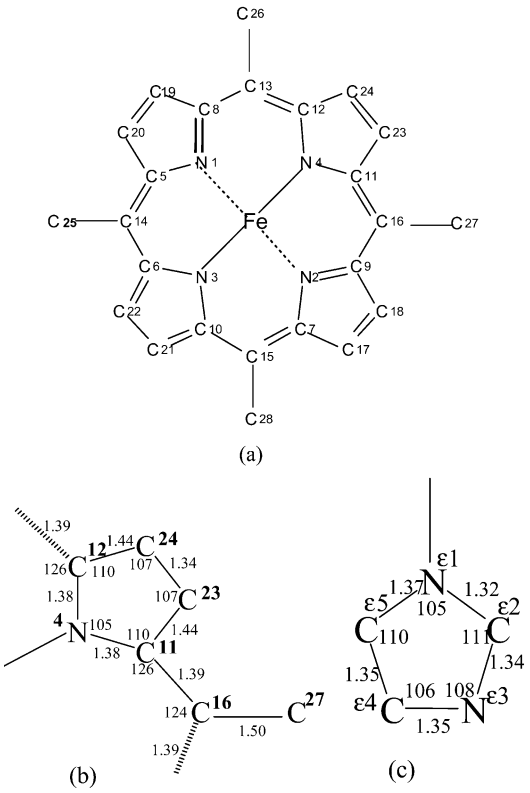

FIGURE 1: (a) Structure of the TPP model used in the MS fits to the XAFS; (b) bond lengths and bond angle restraints used in the pyrrole ring of the TPP model during XAFS analysis; and (c) bond lengths and bond angle restraints used in the histidine ring during XAFS analysis. The designations of the atoms in the model are given in the figure.

includes multiple-scattering codes (*29*, *30*). The goodness-of-fit parameter (*R*) and Monte Carlo calculations were performed as reported previously (*20*, *25*, *29*). The rms errors that result from the Monte Carlo analysis were combined with systematic errors to obtain the final error estimate (*25*). All background subtraction, splining, and normalization procedures were performed using XFIT as reported previously (*20*).

A window from 0 to 16 $Å^{-1}$ with a cosine edge function was applied to the XAFS data. The Fourier transform had a window applied from 0.5 to 5 Å. This window filtered the majority of the atomic XAFS (between 0 and ~1.5 Å), which is difficult to model.

Determinacy. The number of parameters being refined, *p*, compared to the number of independent points, N_i, was calculated to give the degree of determinacy N_i/p. If this ratio is <1, then the model is considered to be underdetermined, and a unique fit is not possible. In all cases, the ratio was >1, and hence the models were overdetermined. The value of N_i is given by (*31*)

$$N_i = 2(\Delta r)(\Delta k)/\pi + \sum[D(N-2)+1] \qquad (1)$$

where *D* is the number of dimensions in which the refinement takes place (two for the planar porphyrin and three for the NO group and free rotation axial group) and *N* is the number of atoms in the unit (*31*). These calculations are combined with different *k* ranges for each compound to give the determinacy values given in the tables.

Table 1: Electronic Absorption Spectral Data for the NO Adducts of Horse Heart Myoglobin (Mb), Soybean Leghemoglobin (Lb), and IDO

protein adduct	λ_{max} (nm)	protein adduct	λ_{max} (nm)	protein adduct	λ_{max} (nm)
$Mb^{II}NO$[a]	422	$Lb^{II}NO$[a]	414	$IDO^{II}NO$[b]	418

[a] See ref *35*. [b] See refs *4* and *6*.

Goodness of Fit (Residual). The method of determining the goodness of fit was through an *R* value, where *R* is given by

$$R = (X^2/X^2_{\text{calculated}=0})^{1/2} \qquad (2)$$

where X^2 is the quantity minimized during the refinement and $X^2_{\text{calculated}=0}$ is the value of X^2 when the calculated XAFS is uniformly 0 (*29*). Residual *R* values of ≤20% were considered reasonable (*31*).

Monte Carlo Error Analysis. Monte Carlo analyses were conducted to estimate the rms deviations in the final parameters arising from the noise in the data. Two consecutive sets of 16 × 16 Monte Carlo cycles were calculated, and the resulting rms errors were combined with systematic errors to determine the final error estimates, as reported previously (*20*, *25*).

RESULTS

Electronic Absorption Spectra. The spectrum of $IDO^{II}NO$ exhibited the expected Soret band at 418 nm (*6*). This is similar to other heme protein NO adducts (Table 1 and Figure S1 in the Supporting Information) (*4*, *6*, *32*).

XANES Analysis. The XANES region of the $IDO^{II}NO$ (Figure 2) is similar to those of [Fe^{II}(TPP)(NO)] (*32*), $Mb^{II}NO$ (*20*), and $Lb^{II}NO$ (*22*). The main difference is in the intensity of the pre-edge peak with the intensity of $IDO^{II}NO$ being closer to the five-coordinate [Fe^{II}(TPP)(NO)] complex than the six-coordinate $Mb^{II}NO$ or $Lb^{II}NO$ adducts. The position and structure of the edge spectrum are sensitive indicators of the photodecomposition of $IDO^{II}NO$. The edge was monitored during the collection of the data, and the effect of irradiation was shown to be negligible for all scans.

MS Analyses of XAFS of $IDO^{II}NO$. In the basic model, the initial bond lengths were Fe−N_p = 1.99 Å, Fe−N_ϵ = 2.0 Å, and Fe−NO = 1.75 Å, with free rotation of the imidazole and NO groups. This gave reasonable final bond lengths (Fe−N_p = 2.01 Å, Fe−N_ϵ = 2.23 Å, and Fe−N_{NO} = 1.76 Å) and Debye−Waller factors (N_p = 0.003 $Å^2$, N_ϵ = 0.003 $Å^2$, and N_{NO} = 0.005 $Å^2$) but yielded unrealistically high residual (24%) and S_0^2 (1.28) values (Table 2 and Table S2 in the Supporting Information). Using a similar starting model in which the initial Fe−N_ϵ bond length was at 2.5 Å, instead of 2.0 Å, resulted in reasonable bond lengths (Fe−N_p = 2.01 Å, Fe−N_ϵ = 2.51 Å, and Fe−N_{NO} = 1.75 Å), Debye−Waller factors (N_p = 0.002 $Å^2$, N_ϵ = 0.01 $Å^2$, and N_{NO} = 0.004 $Å^2$) and a residual value (19.8%) (Table 2 and Table S2 in the Supporting Information). A five-coordinate model, without the imidazole ring, gave a high residual of 30% (Table S2 in the Supporting Information).

Mixed-site models were used to combine the above basic models. The model with the first site having a long Fe−N_ϵ bond length and the second site having a short Fe−N_ϵ bond

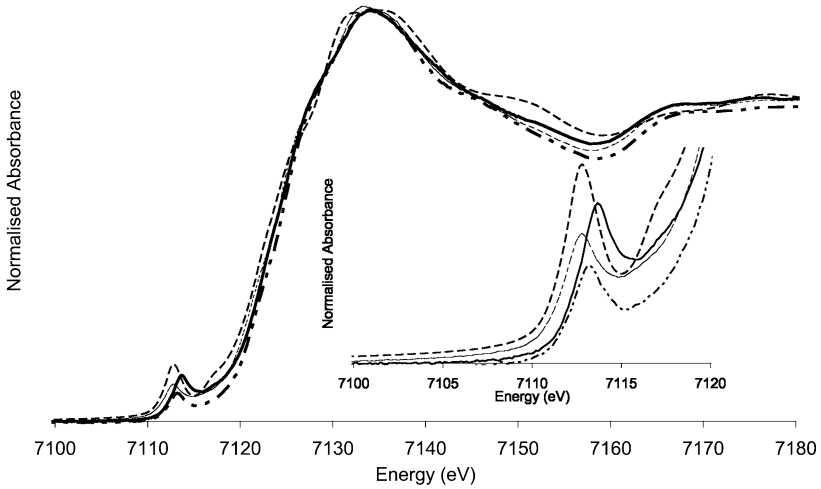

FIGURE 2: K-edge XANES spectra of $IDO^{II}NO$ (—) as compared with $Mb^{II}NO$ (— ••), $Lb^{II}NO$ (- - -), and $[Fe^{II}(TPP)(NO)]$ (- - -) at 10 K.

Table 2: Comparison of Fe−Ligand Dimensions as Determined by MS XAFS Analyses and XRD Structures of NO Adducts of Hemes

		Fe−ligand distances (Å)				angle (deg)	Debye−Waller factors, σ^2 (Å^2)					
heme	method	N_p	N_{ax}	N_{NO}	N−O	Fe−N−O	N_p	N_{ax}	N_{NO}	O_{NO}	S_0^2	R (%)
$Mb^{II}NO$[a]	MS	1.99(2)	2.05(3)	1.76(2)	1.12(2)	150(2)	0.002	0.001	0.005	0.005	0.87	13.8
$Mb^{II}NO$[b]	crystal	2.07	2.18(3)	1.89(4)	1.15	112(5)						
$Lb^{II}NO$[c]	MS	2.02	1.98	1.77	1.12	147	0.003	0.001	0.002	0.007	0.87	16.1
$Lb^{II}NO$[d]	crystal	1.99(7)	2.20(7)	1.72(7)	1.35[e]	147(4)						
$[Fe^{II}(TPP)(NO)]$[a]	MS	2.01(2)		1.74(2)	1.12(2)	155(2)	0.003		0.005		0.99	14.2
$[Fe^{II}(TPP)(NO)]$[f]	crystal	2.001(3)		1.717(7)	1.12(1)	149.2(6)						6.1
$IDO^{II}NO$[g,j]	MS	2.01(2)	2.23(2)	1.76(2)	1.10(2)	146	0.003	0.003	0.005	0.0005	1.28	24.2
$IDO^{II}NO$[h,j]	MS	2.00(2)	2.51(2)	1.75(2)	1.12(2)	144	0.002	0.001	0.004	0.0005	0.96	19.8
$IDO^{II}NO$[i,j]	MS											18.7
$IDO^{II}NO$	MS	2.00(2)	2.51(2)	1.75(2)	1.12(2)	140	0.003	0.0005	0.002	0.002	0.99	
$IDO^{III}NO$	MS	2.00(2)		1.63(3)	1.12(2)	179	0.003		0.017	0.004	0.99	

[a] See ref *20*. [b] Crystal structure of 1.7-Å resolution (*38*). [c] See ref *22*. [d] Crystal structure of 1.8-Å resolution (*39*). [e] The error estimate in L−L bond lengths is uncertain. [f] Crystal structure from Scheidt et al. (*27*). [g] Determinacy = 1.5; short N_{ax}. [h] Determinacy = 1.5; long N_{ax}. [i] Determinacy = 1.15; $IDO^{II}NO$ (70%) and $IDO^{III}NO$ (30%). [j] This paper.

length gave a residual value of 14%. The S_0^2 values were 0.92 (first site) and 1.37 (second site). The N−O bond length was 0.99 Å (first site) and 1.34 Å (second site). The S_0^2 value for the second site and the N−O bond lengths are both too short (first site) and too long (second site) to be chemically reasonable. A model with a short Fe−N_ϵ bond length in the first site and a five-coordinate heme protein as the second site gave a residual value of 20%. The S_0^2 values of 1.28 (first site) and 1.37 (second site) were unacceptably high. The N−O bond length was 1.09 Å (first site) and 1.13 Å (second site) (Table S2 in the Supporting Information). Other models fitted include a water ligand (residual 29%) (Table S2 in the Supporting Information) and a $RCOO^-$ ligand (residual 32%) (Table S2 in the Supporting Information) in the proximal axial site to test the suitability of using the imidazole ring in this position. The best fit to the XAFS data was obtained with a two-site model with a starting distance of 2.5 Å for the proximal axial imidazole ligand in the first site and a second site with a five-coordinate NO heme adduct with the proximal coordination position vacant (Figure 3).

The observed and calculated XAFS, $\chi(k) \times k^3$, the corresponding Fourier transforms, the residuals, $\Delta - [\chi(k) \times k^3]$, and the window functions used in the Fourier filter for the best MS analysis of the $[IDO^{II}NO]$ XAFS data are shown in Figure 4. The distorted six-coordinate model has fitted values for the Fe−N_p(av) bond length = 2.00 Å, the

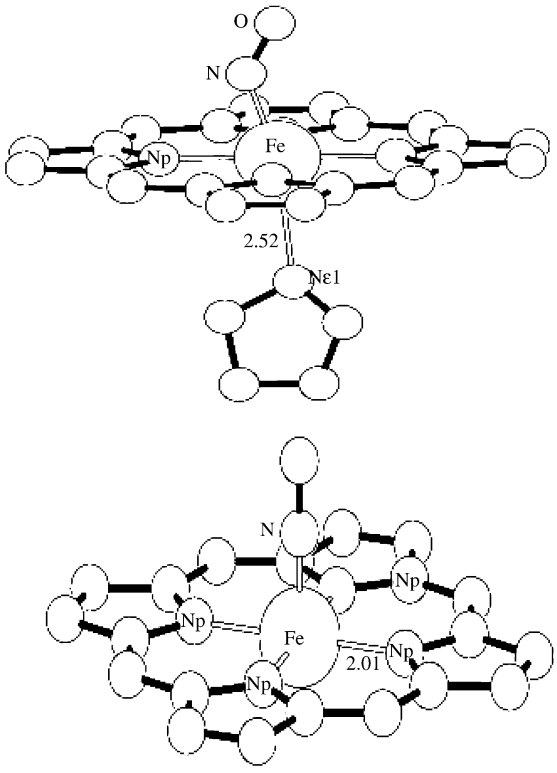

FIGURE 3: XAFS-derived molecular structure of the active site of (a) $IDO^{II}NO$ and (b) $IDO^{III}NO$.

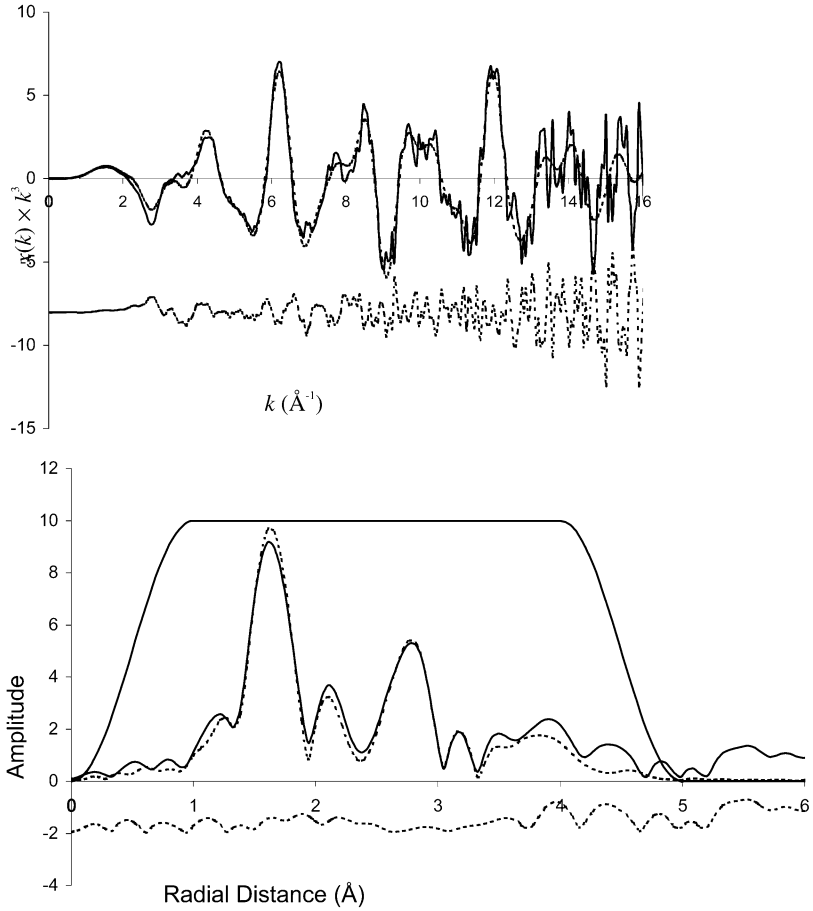

FIGURE 4: (a) XAFS and (b) Fourier transform amplitude of XAFS of IDO−NO at 10 K: observed (—), calculated from the MS two-site model containing IDO^{II}NO (70%) and IDO^{III}NO (30%) model (- - -), residual (— · —), window used in Fourier filter (—), using the two-site model.

Fe−N_ϵ bond length = 2.51 Å, the Fe−N_{NO} bond length = 1.75 Å, and the Fe−N−O bond angle = 140°; the Fe−N_{NO} bond deviates from the normal to the porphyrin by 18°. The occupancy value for this site was 70%. The five-coordinate model gave fitted values of Fe−N_p = 2.00 Å, Fe−N_{NO} = 1.63 Å, and Fe−N−O angle = 179° (Table 2). The paths and importance factors for this analysis are contained in the Supporting Information (Tables S3 and S4 in the Supporting Information). To ensure that these Fe−N−O bond-angle values were not false minima, a second analysis was completed with the starting bond angle of 130° for both sites. The end result was within the error of the initial results, indicating the angles 140° and 179° were not false minima.

DISCUSSION

The Soret band of IDO^{II}NO at 418.5 nm lies between the positions of the Soret bands for Mb^{II}NO and Lb^{II}NO, and the MCD peak and trough positions and intensities for this IDO derivative compare well with analogous Mb proteins (*33*−*35*). The bond angles and lengths are consistent, as expected, with those found in model heme complexes and other heme proteins (*20*, *22*), which provides confidence that the analysis has provided meaningful information on the structures of the heme centers in the Fe^{III} and Fe^{II} adducts.

The one difference in the coordination sphere was a lack of an Fe−N_ϵ bond. The XANES show that the pre-edge peak of IDO^{II}NO is more intense than those of Mb^{II}NO and Lb^{II}NO (or their Fe^{III} analogues) and is closer in intensity to that of [Fe^{II}(TPP)(NO)], a purely five-coordinate structure (Figure 2) (*20*, *22*). This pre-edge feature is due to a symmetry-forbidden 1s → 3d transition, which gains intensity from relaxation of the selection rule because of the mixing of the d and p orbitals. Such mixing is much greater in five-coordinate complexes than octahedral complexes, and thus the XANES is consistent with a significant distortion from an octahedral geometry as a consequence of the long Fe−N_ϵ bond length of 2.44 Å. Thus, the structural information gained from the XANES and XAFS is consistent for both in pointing to a five-coordinate structure for the NO adducts.

For heme proteins such as soluble guanylyl cyclase, the binding of NO weakens or breaks the bond between the heme and the protein (*36*), leading to irreversible activation of the protein. The difference in the case of IDO is that the evidence points to reversible inhibition of IDO by NO binding (*37*). Additional studies are required to elucidate the mechanisms by which NO inhibits IDO in vitro and in vivo, but the results reported here indicate that both blocking of the heme site to O_2 binding and conformational changes induced by breaking the Fe−N_ϵ bond may be important.

The minor five-coordinate site has Fe−NO and Fe−N−O bond angles typical of an Fe^{III}NO adduct (*20*, *22*) and was no doubt a result of the incomplete reduction of this adduct. It shows that the interaction of NO with the met form of the protein also breaks the Fe−N_ϵ bond.

While it is expected that the Fe atom would be displaced out of the heme plane toward the NO group in the five-

coordinate structure, this cannot be reliably assessed when analyzing the two different coordination sites because the XAFS is not very sensitive to out-of-plane displacements (*25*). Similarly, alternative methods of determining out-of-plane displacements using the ratio of peaks in the ligand-field indicator region (*40*) were inappropriate because of the overlap of spectra from two different heme sites.

CONCLUSION

Unlike $Mb^{II}NO$, $Mb^{III}NO$, $Lb^{II}NO$, and $Lb^{III}NO$, $IDO^{II}NO$ and $IDO^{III}NO$ are five-coordinate species with typical Fe−NO bond lengths and angles for Fe−NO species in the appropriate oxidation state. The breaking of the Fe−NO bond may be important in its putative biological function.

ACKNOWLEDGMENT

We are grateful to the invaluable assistance provided by Professor Keith Hodgson, Dr. Britt Hedman, Dr. Ingrid Pickering, Dr. Paola de Cecco, and Dr. Mathew Latimer at SSRL and Jacinta Letters at the Heart Research Institute.

SUPPORTING INFORMATION AVAILABLE

Table S1, constraints and restraints used in MS XAFS analysis using the TPP model for the porphyrin; Table S2, the effect of the varying input model on the fitted result for IDO−NO; Table S3, paths and importance factors from the MS analysis using the mixed-site; model for the MS refinement of the XAFS of IDO^{II}−NO (10 K), distorted six-coordinate IDO site; and Table S4, paths and importance factors from the MS analysis using the mixed-site model for the MS refinement of the XAFS of IDO^{III}−NO (10 K), five-coordinate IDO site. This material is available free of charge via the Internet at http://pubs.acs.org.

REFERENCES

1. Hayaishi, O. (1985) Indoleamine 2,3-dioxygenase—with special reference to the mechanism of interferon action, *Biken J. 28*, 39−49.
2. Sun, Y. (1989) Indoleamine 2,3-dioxygenase—a new antioxidant enzyme, *Mater. Med. Pol. Engl. Ed. 21*, 244−250.
3. Taylor, M. W., and Feng, G. (1991) Relationship between interferon-γ, indoleamine 2,3-dioxygenase and tryptophan catabolism, *FASEB J. 5*, 2516−2522.
4. Sono, M., Taniguchi, T., Watanabe, Y., and Hayaishi, O. (1980) Indoleamine 2,3-dioxygenase—equilibrium studies of the tryptophan binding to the ferric, ferrous and co-bound enzymes, *J. Biol. Chem. 255*, 1339−1345.
5. Sono, M. (1989) The roles of superoxide anion and methylene blue in the reductive activation of indoleamine 2,3-dioxygenase by ascorbic acid or by xanthine oxidase-hypoxanthine, *J. Biol. Chem. 264*, 1616−1622.
6. Sono, M., and Dawson, J. H. (1984) Extensive studies of the heme coordination structure of indoleamine 2,3-dioxygenase and of tryptophan binding with magnetic and natural circular dichroism and electron paramagnetic resonance spectroscopy, *Biochim. Biophys. Acta 789*, 170−187.
7. Sono, M. (1990) Spectroscopic and equilibrium studies of ligand and organic substrate binding to indoleamine 2,3-dioxygenase, *Biochemistry 29*, 1451−1460.
8. Hirata, F., Ohnishi, T., and Hayaishi, O. (1977) Indoleamine 2,3-dioxygenase. Characterisation and properties of enzyme·O_2^- complex, *J. Biol. Chem. 252*, 4637−4642.
9. Terentis, A. C., Thomas, S. R., Takikawa, O., Littlejohn, T. K., Truscott, R. J. W., Armstrong, R. S., Yeh, S.-R., and Stocker, R. (2002) The heme environment of recombinant human indoleamine 2,3-dioxygenase. Structural properties and substrate-ligand interactions, *J. Biol. Chem. 277*, 15788−15794.
10. Thomas, S. R. (1998), Ph.D. Thesis, University of Sydney, Sydney, Australia.
11. Thomas, S. R., Witting, P. K., and Stocker, R. (1996) 3-Hydroxyanthranilic acid is an efficient, cell-derived co-antioxidant for a-tocopherol, inhibiting human low-density lipoprotein and plasma lipid peroxidation, *J. Biol. Chem. 271*, 32714−32721.
12. Thomas, S. R., Mohr, D., and Stocker, R. (1994) Nitric oxide inhibits indoleamine 2,3-dioxygenase activity in interferon-γ primed mononuclear phagocytes, *J. Biol. Chem. 269*, 14457−14464.
13. Antonini, E., and Brunori, M. (1971) *Hemoglobin and Myoglobin in Their Reactions with Ligands*, North-Holland, Amsterdam.
14. Armstrong, R. S., Irwin, M. J., and Wright, P E. (1980) Resonance Raman evidence for constrained heme structure in soybean leghemoglobin and its derivatives, *Biochem. Biophys. Res. Commun. 95*, 682−689.
15. Irwin, M. J., Armstrong, R. S., and Wright, P. E. (1981) Resonance Raman studies of soybean leghemoglobin and myoglobin, *FEBS Lett. 133*, 239−243.
16. Narula, S. S., Dalvit, C., Appleby, C. A., and Wright, P. E. (1988) NMR studies of the conformations of leghemoglobins from soybean and lupin, *Eur. J. Biochem. 178*, 419−435.
17. Ignaro L. J. (1999) Nitric oxide as a signaling molecule in the vascular system: an overview, *J. Cardiovasc. Pharmacol. 34*, 879−886.
18. Ribeiro, J. M. C., Hazzard, J. M. H., Nussenzveig, R. H., Champagne, D. E., and Walker, F. A. (1993) Reversible binding of nitric oxide by a salivary heme protein from a bloodsucking insect, *Science 260*, 539−541.
19. Jia, L., Bonaventura, C., Bonaventura, J., and Stamler, J. S. (1996) *S*-Nitrosohaemoglobin: a dynamic actvity of blood involved in vascular control, *Nature 380*, 221−226.
20. Rich, A. M., Armstrong, R. S., Ellis, P. J., and Lay, P. A. (1998) Determination of the Fe−ligand bond lengths and Fe−N−O bond angles in horse heart ferric and ferrous nitrosylmyoglobin using multiple-scattering XAFS analyses, *J. Am. Chem. Soc. 120*, 10827−10836.
21. Stynes, D. V., Stynes, H. C., James, B. R., and Ibers, J. A. (1973) Reversible binding of nitric oxide and carbon monoxide to iron porphyrins. Assessment of the role of the protein in hemoglobin, *J. Am. Chem. Soc. 95*, 4087−4089.
22. Rich, A. M., Ellis, P. J., Tennant, L., Wright, P. E., Armstrong, R. S., and Lay, P. A. (1999) Determination of Fe−ligand bond lengths and the Fe−N−O bond angles in soybean ferrous and ferric nitrosylleghemoglobin *a* using multiple-scattering XAFS analyses, *Biochemistry 38*, 16491−16499.
23. Littlejohn, T. K., Takikawa, O., Skylas, D., Jamie, J. F., Walker, M. J., and Truscott, J. W. (2000) Expression and purification of recombinant human indoleamine 2,3-dioxygenase, *Protein Expression Purif. 19*, 22−29.
24. Arnold, E. V., and Bohle, D. S. (1996) Isolation and oxygenation reactions of nitrosylmyoglobins, *Methods Enzymol. 269*, 41−48.
25. Rich, A. M., Armstrong, R. S., Ellis, P. J., Freeman, H. C., and Lay, P. A. (1998) Determination of iron−ligand bond lengths in horse heart met- and deoxymyoglobin using multiple-scattering XAFS analyses, *Inorg. Chem. 37*, 5743−5753.
26. Wyllie, G. R. A., and Scheidt, W. R. (2003) NO orientation and tilting in (nitrosyl)iron(II) deuterioporphyrin IX, *Inorg. Chem. 42*, 4259−4261.
27. Scheidt, W. R., and Frisse, M. E. (1975) Nitrosylmetalloporphyrins. II. Synthesis and molecular stereochemistry of nitrosyl-$\alpha,\beta,\gamma,\delta$-tetraphenylporphinatoiron(II), *J. Am. Chem. Soc. 97*, 17−21.
28. Penner-Hahn, J. E. (1999) X-ray absorption spectroscopy in coordination chemistry, *Coord. Chem. Rev. 190−192*, 1101−1123.
29. Ellis, P. J., and Freeman, H. C. (1995) XFIT—an interactive EXAFS analysis program, *J. Synchrotron Radiat. 2*, 190−195.
30. Zabinsky, S. I., Rehr, J. J., Ankudinov, A., Albers, R. C., and Eller, M. J. (1995) Multiple-scattering calculations of X-ray absorption spectra, *Phys. Rev. B: Condens. Matter 52*, 2995−3009.
31. Bianconi, A., Dell'Ariccia, M., Durham, P. J., and Pendry, J. B. (1982) Multiple-scattering resonances and structural effects in the X-ray absorption near-edge spectra of Fe^{II} and Fe^{III} hexacyanide complexes, *Phys. Rev. B: Condens. Matter 26*, 6502−6508.

32. Rich, A. M. (1997), Ph.D. Thesis, University of Sydney, Sydney, Australia.
33. Fasman, G. D. (1976) *Handbook of Biochemistry and Molecular Biology, Proteins*, 3rd ed., Vol. 2, CRC Press, Cleveland, OH.
34. Antonini, E. (1965) Interrelationship between structure and function in hemoglobin and myoglobin, *Physiol. Rev. 45*, 123−170.
35. Appleby, C. A. (1974) *The Biology of Nitrogen Fixation*, North-Holland, Amsterdam.
36. Dierks, E. A., Hu, S., Vogel, K. M., Yu, A. E., Spiro, T. G., and Burstyn, J. N. (1997) Demonstration of the role of scission of the proximal histidine-iron bond in the activation of soluble guanylyl cyclase through metalloporphyrin substitution studies, *J. Am. Chem. Soc. 119*, 7316−7323.
37. Thomas, S. R., and Stocker, R. (1999) Redox reactions related to indoleamine 2,3-dioxygenase and tryptophan metabolism along the kynurenine pathway, *Redox Rep. 4*, 199−220.
38. Brucker, E. A., Olson, J. S., Ikeda-Saito, M., and Phillips, G. N., Jr. (1998) Nitric oxide myoglobin: Crystal structure and analysis of ligand geometry, *Proteins: Struct., Funct., Genet. 30*, 352−356.
39. Harutunyan, E. H., Safonova, T. N., Kuranova, I. P., Popov, A. N., Teplyakov, A. V., Obmolova, G. V., Vainshtein, B. K., Dodson, G. G., and Wilson, J. C. (1996) The binding of carbon monoxide and nitric oxide to leghaemoglobin in comparison with other haemoglobins, *J. Mol. Biol. 264*, 152−161.
40. Chance, M. R., Parkhurst, L. J., Powers, L. S., and Chance, B. (1986) Movement of Fe with respect to the heme plane in the R−T transition of carp hemoglobin. An extended X-ray absorption fine structure study, *J. Biol. Chem. 261*, 5689−5692.

BI049645S